Macroscopic Modelling of Rough Wall Turbulence Based on the Second Moment Closure

doi: https://doi.org/10.1615/THMT-18.380

Turbulence, Heat and Mass Transfer 9

Macroscopic Modelling of Rough Wall Turbulence Based on the Second Moment Closure

Y. Kuwata[1], K. Suga[1] and Y. Kawaguchi[2]

[1] *Department of Mechanical Engineering, Osaka Prefecture University, Sakai, Osaka 599-531, Japan. kuwata@osakafu-u.ac.jp*

[2] *Department of Mechanical Engineering, Tokyo University of Science, Noda, Chiba 278-8510, Japan.*

Abstract — To predict rough wall turbulence without resolving rough geometry, spatial and Reynolds (double) averaged equations are modelled based on the two-component limit (TCL) second moment closure. The additional terms, namely, double averaged drag force and inhomogeneous correction terms arise due to the double averaging process. The double averaged drag force is modelled as the Darcy-Forchheimer form, and binomial expansion is applied to model the effects of fluctuating velocity on the double averaged drag force. The influence of the drag force on a pressure-strain term is modelled with TCL constraints. The developed model is calibrated in turbulence over randomly distributed semi-spheres and spray paint surfaces. The modifications of the skin friction in transitionally and fully rough regimes is confirmed to be successfully predicted by the developed model.

1. Introduction

Most wall surfaces encountered in geophysical and engineering flows cannot be regarded as hydraulically smooth. In engineering context, the wall roughness is inevitably occurred in production processes due to imperfections of surface finishing. Furthermore, erosion or corrosion by aging, and fouling processes makes the surface rough, e.g., aerodynamic flows over airfoils with icing, ship hull roughness due to organic fouling or turbine blade eroded by impinging combustor air. Since the wall-roughness causes degradation of the machine performance due to an increase in skin friction, accurate and reliable prediction of rough wall turbulence are of great important issues in many engineering design.

The most primitive approach to account for roughness shape was including the blockage and drag force effects of roughness elements to the mixing length turbulence model [1, 2]. However, since the model validation was limited to flows over rib-type roughness, the model had a narrow range of applicability for the other types of rough surfaces. For more elaborate approach, an extension for the two-layer $k-\varepsilon$ model was made by [3]. They modified the eddy viscosity vicinity of the rough wall by introducing hydrodynamic roughness length scale and changed the boundary conditions for the turbulence energy at the rough wall. Modification of the wall-boundary conditions for k and ω depending on the roughness Reynolds number was also made by [4]. In a similar approach, [5] extended the Spalart-Allmaras model assuming a non-zero-eddy viscosity at the wall and changing the wall-normal distance to mimic roughness effect. Comparison with experiments for sand papers, reproduced aged turbine blades and staggered array of spheres confirmed general agreement of the rough wall skin friction. Although many other important attempts on modelling the rough wall turbulence can be found in the literature, most of the approaches were merely modified the wall-boundary condition based on the empirical correlation of [6]. Furthermore, since all models have established by using the equivalent roughness, those are incapable of applying turbulent flows over the naturally occurring rough walls whose equivalent roughness is usually unknown.

Another idea to model flows within complex structures such as porous media is employing the spatial averaged equations [7, 8]. Recently, to demonstrate effectiveness of this approach for rough wall turbulence, the present authors simulated turbulence over rough walls by solving spatial averaged equation in the rough wall region, and we confirmed that an influence of rough surfaces on turbulence could be reasonably captured by solving the spatial averaged equation with a simple drag force model [9]. Accordingly, the present study extends this approach by further applying the Reynolds averaging in addition to the spatial averaging, and attempts to macroscopically model turbulence within rough walls without using the equivalent roughness and the empirical correlation of [6]

2. Double-averaged Navier-Stokes equations

In order to statistically treat flows around roughness elements where the mean flows become spatially inhomogeneous due to the presence of the roughness elements, the spatial averaging is considered. Following [9], the representative elementary plane (REP) which is parallel to the rough wall is introduced for the spatial averaging. The definition of the superficial plane averaging of ϕ is introduced as

$$\langle \phi \rangle = \frac{1}{A_S} \int_S \phi dS, \tag{1}$$

where S and A_S denote a representative elementary plane of the spatial averaging and plane area of S, respectively. A variable ϕ can be decomposed into contribution from an intrinsic (fluid phase) averaged value: $\langle \phi \rangle^f$:

$$\langle \phi \rangle^f = \frac{1}{A_{S_f}} \int_S \phi dS, \tag{2}$$

and deviation from the intrinsic averaged value: $\tilde{\phi}$ as

$$\phi = \langle \phi \rangle^f + \tilde{\phi}, \tag{3}$$

where A_{S_f} denotes plane area of fluid phase contained within S, and a relation exists between the superficial and intrinsic plane-averaged values as: $\langle \phi \rangle = \varphi \langle \phi \rangle^f$. Here, the plane porosity φ is defined as $\varphi = A_S / A_{S_f}$ To model turbulent flows over rough walls, the Reynolds decomposition is also introduced a as

$$\phi = \overline{\phi} + \phi', \tag{4}$$

where $\overline{\phi}$ is the Reynolds averaged value and ϕ' denotes its fluctuation.

Applying the plane and Reynolds (double) averaging to the momentum equation for incompressible flows, the double averaged momentum equation can be written as

$$\begin{aligned} \frac{\partial \langle \overline{u}_i \rangle^f}{\partial t} + \frac{\partial \langle \overline{u}_j \rangle^f \langle \overline{u}_i \rangle^f}{\partial x_j} = & -\frac{1}{\rho} \frac{\partial \langle \overline{p} \rangle^f}{\partial x_i} + \frac{1}{\varphi} \frac{\partial}{\partial x_j} \left(\nu \frac{\partial \varphi \langle \overline{u}_i \rangle^f}{\partial x_j} \right) \\ & - \frac{1}{\varphi} \frac{\partial}{\partial x_j} \varphi \left(\underbrace{\langle \overline{u_i' u_j'} \rangle^f}_{R_{ij}^A} + \underbrace{\langle \tilde{\overline{u}}_i \tilde{\overline{u}}_j \rangle^f}_{\mathcal{T}_{ij}} \right) - \underbrace{\frac{\nu}{\varphi} \frac{\partial \varphi}{\partial x_j} \frac{\partial \langle \overline{u}_i \rangle^f}{\partial x_j}}_{\overline{g}_i^{\varphi}} - \overline{f}_i \end{aligned} \tag{5}$$

where, R_{ij}^A and $\mathcal{T}_{ij}$ are the plane-averaged Reynolds stress and the plane-dispersive covariance, respectively. Here, $\tilde{u}$ is the velocity dispersion defined as: $\tilde{u} = u - \langle u \rangle^f$. The plane averaged

Reynolds stress is obtained by solving their transport equations while $\mathcal{T}_{ij}$ is neglected in the present model because its contribution is marginal compared with the other stress terms [9]. The inhomogeneous correction term $\overline{g}_i^{\varphi}$ arise due to the spatial inhomogeneity of φ. The term f_i is the plane-averaged drag force term, which consists of the pressure and viscous drag terms, and it is modelled as in [9]:

$$f_i = \nu C_1^D \langle u \rangle_i^f + C_2^D \langle u_i \rangle^f \sqrt{\langle u_k \rangle^f \langle u_k \rangle^f}, \tag{6}$$

where C_1^D and C_2^D are the dimensional model functions which are expressed as the function of the plane-hydraulic diameter D_m and φ as

$$C_1^D = \frac{2C_1}{\pi} \frac{(1-\varphi)}{\varphi^2 D_m^2}, \quad C_2^D = \frac{2C_2}{\pi} \frac{(1-\varphi)}{\varphi^{2.5} D_m}, \tag{7}$$

where the model constants $C_1 = 71$ and $C_2 = 0.79$ are presently used.

When we apply the Reynolds averaging to Eq.(6), the second term on the right-hand-side of Eq.(6) can be written as

$$\overline{\langle u_i \rangle^f \sqrt{(\langle u_k \rangle^f)^2}} = \overline{\left(\langle \bar{u}_i \rangle^f + \langle u_i' \rangle^f \right) \left\{ \left(\langle \bar{u}_k \rangle^f \right)^2 + 2 \langle \bar{u}_k \rangle^f \langle u_k' \rangle^f + \left(\langle u_k' \rangle^f \right)^2 \right\}^{1/2}}, \tag{8}$$

Since the Reynolds averaged form could not be strictly expanded, then, [10] assumed that $\left(\langle \bar{u}_k \rangle^f \right)^2 >> \left(\langle u_k' \rangle^f \right)^2$ and applied the binomial series expansion to $\left\{ \left(\langle \bar{u}_k \rangle^f \right)^2 + 2 \langle \bar{u}_k \rangle^f \langle u_k' \rangle^f \right\}^{1/2}$ as

$$\begin{aligned} \left\{ \left(\langle \bar{u}_k \rangle^f \right)^2 + 2 \langle \bar{u}_k \rangle^f \langle u_k' \rangle^f \right\}^{1/2} = \left\{ \left(\langle \bar{u}_k \rangle^f \right)^2 \right\}^{1/2} \Bigg[1 + \frac{\langle \bar{u}_l \rangle^f \langle u_l \rangle^{f'}}{\left(\langle \bar{u}_m \rangle^f \right)^2} \\ - \frac{1}{2} \left\{ \frac{\langle \bar{u}_l \rangle^f \langle u_l' \rangle^f}{\left(\langle \bar{u}_m \rangle^f \right)^2} \right\}^2 + \frac{1}{2} \left\{ \frac{\langle \bar{u}_l \rangle^f \langle u_l' \rangle^f}{\left(\langle \bar{u}_m \rangle^f \right)^2} \right\}^3 \cdots \Bigg]. \end{aligned} \tag{9}$$

Since the double averaged drag force $\overline{f}_i$ can be

$$\overline{f}_i = \nu C_1^D \langle \overline{u}_i \rangle^f + C_2^D \left(\langle \overline{u}_i \rangle^f \sqrt{\langle \overline{u}_k \rangle^f \langle \overline{u}_k \rangle^f} + \frac{\langle \overline{u}_k \rangle^f}{\sqrt{\langle \overline{u}_l \rangle^f \langle \overline{u}_l \rangle^f}} R_{ik}^A \right), \tag{10}$$

2.1. Modelling the Reynolds stress

The plane-averaged Reynolds stress $R_{ij}^A = \langle \overline{u_i' u_j'} \rangle^f$ can be decomposed into two parts:

$$R_{ij}^A = \langle \overline{u_i' u_j'} \rangle^f = \underbrace{\overline{\langle u_i' \rangle^f \langle u_i' \rangle^f}}_{R_{ij}} + \underbrace{\langle \overline{\tilde{u}_i' \tilde{u}_j'} \rangle^f}_{r_{ij}} \tag{11}$$

where R_{ij} and r_{ij} denote the contributions by the macro-scale velocity fluctuation and the plane-dispersive velocity fluctuation, respectively. Since Kuwata and Kawaguchi [9] reported that momentum transfer contribution by r_{ij} was far smaller than that by R_{ij}, the present study assumes $R_{ij}^A \approx R_{ij}$ and the transport equation of R_{ij} is considered.

The transport equation of R_{ij} may be written as

$$\frac{\partial R_{ij}}{\partial t} + \langle \overline{u_k} \rangle^f \frac{\partial R_{ij}}{\partial x_k} = \mathcal{D}_{ij} + \Pi_{ij} + P_{ij} - F_{ij} + G_{ij}^{\varphi} - \varepsilon_{ij}, \tag{12}$$

The terms $\mathcal{D}_{ij}$, Π_{ij}, P_{ij}, F_{ij}, G_{ij}^{φ} and ε_{ij} are the diffusion, pressure-correlation, mean shear production, drag force, inhomogeneous correction and dissipation rate terms. The drag force and inhomogeneous correction terms are respectively written as

$$G_{ij}^{\varphi} = -\frac{\nu}{\varphi}\frac{\partial \varphi}{\partial x_k}\frac{\partial R_{ij}}{\partial x_k}, \tag{13}$$

$$F_{ij} = 2\nu C_1^D R_{ij} + \frac{C_2^D \langle \overline{u}_k \rangle^f}{\sqrt{\langle \overline{u}_m \rangle^f \langle \overline{u}_m \rangle^f}} \left(2\langle \overline{u}_k \rangle^f R_{ij} + \langle \overline{u}_i \rangle^f R_{jk} + \langle \overline{u}_j \rangle^f R_{ik} - c\tau R_{kl}\frac{\partial R_{ij}}{\partial x_l} \right). \tag{14}$$

where τ is the turbulent time scale: $\tau = k/\varepsilon$, and the model constant $c = 0.22$ is applied. Here, the turbulent kinetic energy is $k = R_{kk}/2$. As presented by Craft and Launder [12], TCL constraints are applied to model the pressure-correlation due to the drag force. The resultant form of $\phi_{ij,3}$ can be written as

$$\begin{aligned}
\phi_{ij,3} = & -\left(\frac{4}{10} + \frac{3}{80}A_2\right)\left(-F_{ij} + \frac{1}{3}F_{kk}\delta_{ij}\right) - \frac{1}{4}a_{ij}F_{kk} \\
& -\frac{1}{20}\left(F_{im}\frac{R_{mj}}{k} + F_{jm}\frac{R_{mi}}{k} + \delta_{ij}\frac{R_{mn}}{k}F_{mn}\right) \\
& -\frac{1}{10}\left(\frac{R_{mn}}{k}\frac{R_{mj}}{k}F_{in} + \frac{R_{mn}}{k}\frac{R_{mi}}{k}F_{jn} - \frac{1}{4}\delta_{ij}\frac{R_{mn}}{k}\frac{R_{nl}}{k}F_{lk}\right) \\
& +\frac{1}{16}\left(\frac{R_{mi}}{k}\frac{R_{nj}}{k}F_{mn} + \frac{R_{mj}}{k}\frac{R_{ni}}{k}F_{mn} + 2\frac{R_{ij}}{k}\frac{R_{mn}}{k}F_{mn}\right),
\end{aligned} \tag{15}$$

where A_2 is the second invariant of the Reynolds stress tensor: $a_{ij} = (R_{ij} - 2/3\delta_{ij})/k$. For the transport equation for the isotropic part of ε_{ij}, the trace of the additional terms F_{kk} and G_{kk}^{φ} are added by dividing the turbulent time scale τ. For the other terms which need modelling, the TCL second moment closure of [11] is applied.

2.2. Modelling the energy dissipation

The transport equation of $\tilde{\varepsilon}(= \varepsilon - 2\nu(\partial\sqrt{k}/\partial x_k)^2)$ can be written as

$$\begin{aligned}
\frac{\partial \tilde{\varepsilon}}{\partial t} + \langle \overline{u}_k \rangle^f \frac{\partial \tilde{\varepsilon}}{\partial x_k} = \frac{\partial}{\partial x_k}\left\{ \left(\nu\delta_{kl} + 0.18R_{kl}\tau\right)\frac{\partial \tilde{\varepsilon}}{\partial x_l} \right\} & + c_{\varepsilon 1}\frac{P_{kk} + G_{kk}^{\varphi}}{2\tau} - c_{\varepsilon 2}\frac{\tilde{\varepsilon}}{\tau} \\
& - \frac{\varepsilon - \tilde{\varepsilon}}{\tau} + P_{\varepsilon 3} + F_{\varepsilon},
\end{aligned} \tag{16}$$

where $c_{\varepsilon 1} = 1.44, c_{\varepsilon 2} = 1.92$ and the influence of the inhomogeneous correction term G_{kk} is added by dividing the turbulence time scale. The drag force term is modelled as

$$F_{\varepsilon} = -2\nu c_{f\varepsilon 1} C_1^D \tilde{\varepsilon} - c_{f\varepsilon 2}\frac{C_2^D \langle \overline{u}_k \rangle^f}{\sqrt{\langle \overline{u}_m \rangle^f \langle \overline{u}_m \rangle^f}} \left(2\langle \overline{u}_k \rangle^f \tilde{\varepsilon} + \frac{\langle \overline{u}_j \rangle^f R_{jk}}{\tau} - cR_{kl}\frac{\partial k}{\partial x_l} \right), \tag{17}$$

where the model coefficients are given as $c_{f\varepsilon 1} = 2.3\exp\left(-(R_t/25)^2\right), c_{f\varepsilon 2} = 0.6$. Here, R_t denotes the turbulent Reynolds number: $R_t = k^2/(\nu\varepsilon)$.

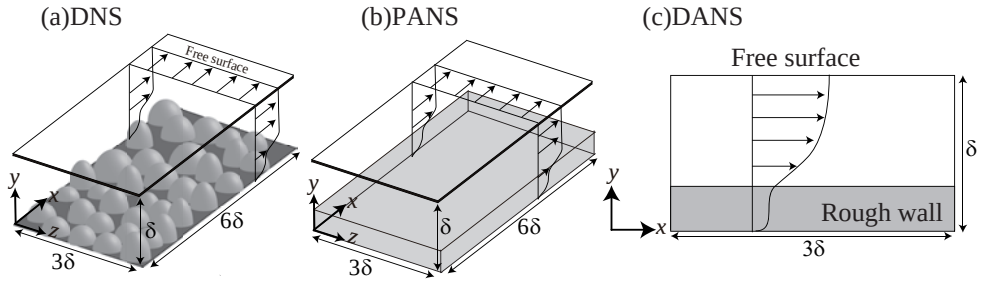

Figure 1: Computational geometry of rough-walled open channel flows: (a)DNS (Direct numerical simulation), (b) PANS (plane-averaged Navier-Stokes), (c) DANS (Double averaged Navier-Stokes).

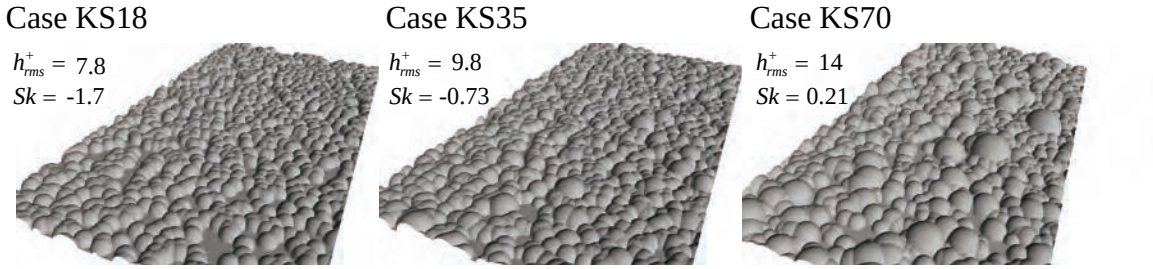

Figure 2: Randomly distributed semi-spheres: (a) KS18, (b) KS35, (c) KS70.

3. Model calibration

The developed model is evaluated in turbulent open-channel flows over two types of rough walls, namely, randomly distributed semi-spheres and spray paint rough surfaces. The predicted results are compared with the direct numerical simulation results of turbulence over randomly distributed semi-spheres in transitional rough regime [9] while the comparison with the experimental data for turbulence over paint rough surfaces in fully-rough regime [13] is made.

3.1. Randomly distributed semi-spheres

The first model calibration is performed in turbulence over the randomly distributed semi-spheres as shown in Fig.1. The predicted results solving the DANS (double-averaged Navier-Stokes) are compared with the results of DNS and PANS (plane-averaged Navier-Stokes) simulation which macroscopically simulates three-dimensional time dependent flows in the rough wall region solving the plane-averaged Navier-Stokes in the rough wall region [9]. Simulations are performed at the constant friction Reynolds number of $\mathrm{Re}_\tau = 300$. The non-uniform meshes presently used have 120 nodes across the channel which is confirmed to be fine enough for grid independent solutions by comparing with the results of twice dense meshes. For the rough walls, the randomly distributed semi-spheres with different equivalent roughness of $k_s^+ = 18, 35$ and 70 which are respectively referred as KS18, KS35 and KS70 as shown in Fig.2 are tested. Note that the values of $k_s^+ = 18, 35$ and 70 indicates that flows are all in the transitionally rough regimes.

Figure 3 compares the superficial plane-averaged streamwise mean velocity profiles. The steramwise mean velocity near the rough wall is significantly damped due to the drag force and the mean velocity away from the rough wall shifts downward with increasing the equivalent roughness k_s^+ which is due to an increase in skin friction coefficient C_f. The predicted mean velocity by the present model (DANS) agree well with the DNS and PANS results. Also, the

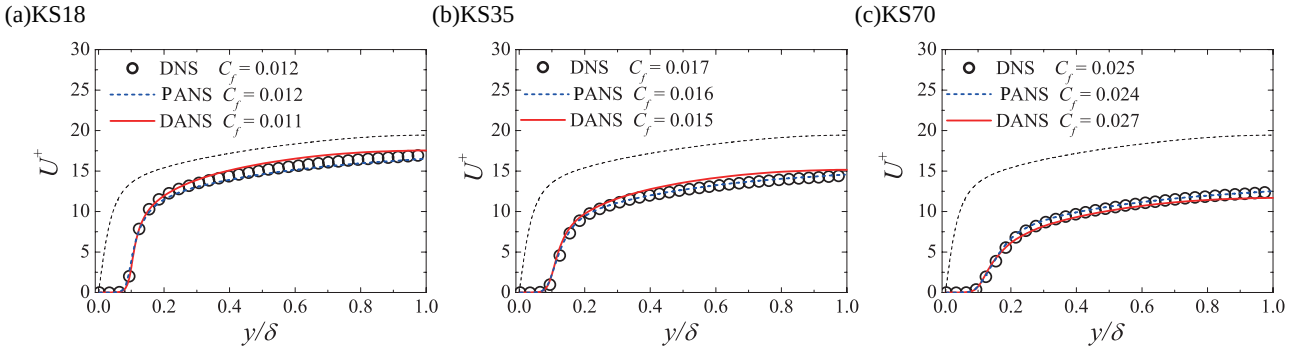

Figure 3: Comparison of superficial plane-averaged streamwise mean velocity profiles: (a) KS18, (b) KS35, (c) KS70.

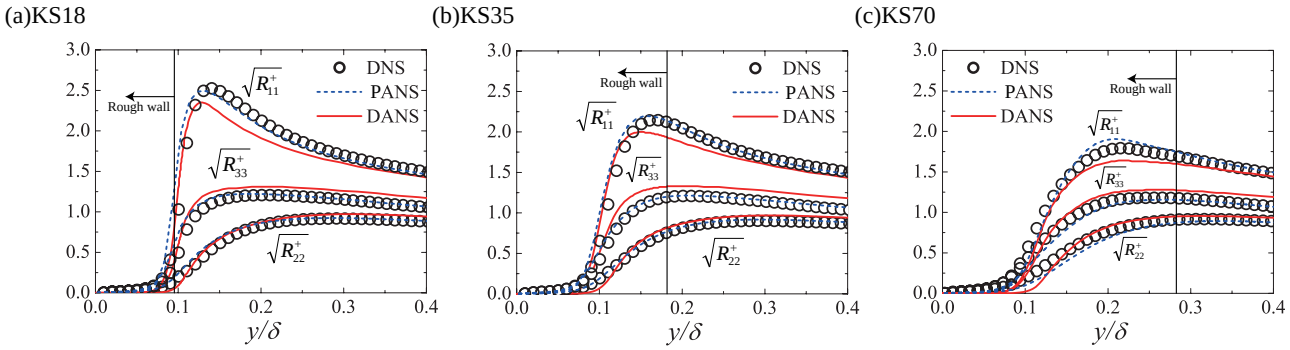

Figure 4: Comparison of superficial plane-averaged Reynolds normal stress profiles : (a) KS18, (b) KS35, (c) KS70.

skin friction coefficient predicted by the present model also show good agreement with the DNS results. Difference in C_f between the DANS and DNS is 10% at most (case KS18). This confirms that the developed model can successfully reproduce the increase in skin friction.

The superficial plane-averaged Reynolds normal stress profiles are compared in Figure 4. Location of the maximum roughness height is also shown. The Reynolds stresses are damped due to the drag force effect inside the rough wall region. As k_s^+ increases, the damping effect tends to be more relaxed and turbulence can penetrate deeply inside the rough wall. The maximum peak of the streamwise component is significantly reduced with increasing k_s^+ while the other components do not change so much. Those trends are reasonably captured by the developed model. However, it is confirmed in Fig.4(c) that the present model underpredict turbulence deeply inside the rough wall of $y/\delta < 0.1$.

3.2. Spray marine paint rough surfaces

The second calibration is performed in turbulence over spray marine paint rough surfaces (case P1, P2, P3 and P4) as shown in Fig.5. The rough walls have almost the same root-mean-square height h_{rms} but significant difference in the skewness Sk. The positive and negative Sk indicates the peak-dominated and valley-dominated rough surfaces, respectively. The rough wall of case P1 has sharp peaks while the rough wall of case P2 has rounded peaks which are both characterized by the positive Sk. The rough wall in case P3, in contrast, has the intermittent deep valley which is characterized by the negative Sk. Simulations are performed at the bulk mean Reynolds number of $\mathrm{Re}_b = 10^5 \sim 10^6$ which corresponds to the fully-rough regimes

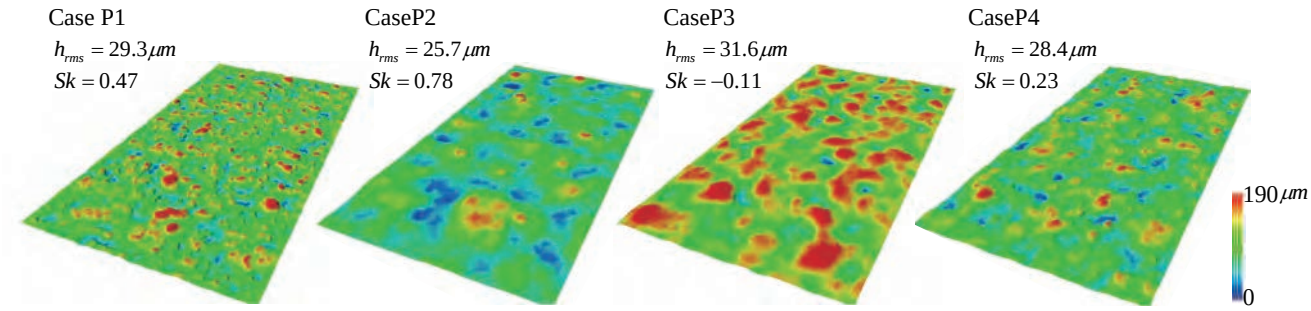

Figure 5: Paint rough surfaces.

because the equivalent roughness varies in the range of $k_s^+ = 200 \sim 6,000$. For the comparison with the experimental data, the half channel height is set to 5.0mm. The non-uniform meshes presently used have 120 nodes across the channel which is confirmed to be fine enough for grid independent solutions by comparing with the results of twice dense meshes.

Figure 6 presents the roughness function ΔU^+ versus k_s^+. The roughness function is the downward shift of the streamwise mean velocity scaled with the friction velocity:

$$U^+ = \frac{1}{\kappa} ln(y^+) + B - \Delta U^+, \tag{18}$$

where κ and B respectively denote the Kármán constant and the log-law intercept for a smooth wall. The equivalent roughness k_s/δ, which takes a unique value depending on the rough surface topology, is determined by fitting ΔU^+ in case of $\mathrm{Re}_b = 10^5$ to the following relation ship [6] in the fully rough regime:

$$B - \Delta U^+ \frac{1}{\kappa} ln(k_s^+) = 8.5. \tag{19}$$

It is confirmed in Fig.6 that all data reasonably collapse well to the correlation of Eq.(19) indicating that the Reynolds number dependence of the roughness function in the fully rough regime is successfully predicted by the present model.

To evaluate the predicted skin friction coefficient, Fig.7 compares the skin friction increasing ratio: C_f/C_{f0} at $\mathrm{Re}_c = 25,000$ with the experimental data of [13]. Here, Re_c is the Reynolds number based on the mean velocity at the slip wall and C_{f0} denotes the skin friction coefficient in a smooth wall case. Note that since the experimental values were obtained in the Taylor - Couette flow whose inner wall was made of the rough wall, the quantitative comparison may not be meaningless; however the trend of C_f/C_{f0} can be worthwhile to compare. The experimental data suggests that C_f/C_{f0} in case P1 takes a maximum value and C_f/C_{f0} in cases P2, P3 and P4 take almost the same values despite the significant difference of the rough surface structures as shown in Fig.5. It is confirmed that the predicted C_f/C_{f0} shows the same trends which suggests that the present model can reasonably predict increase in skin friction at real rough surfaces.

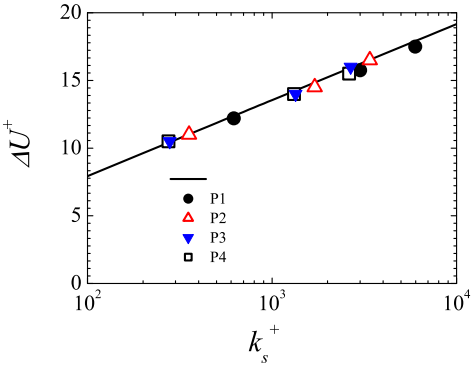

Figure 6: Equivalent roughness versus roughness function.

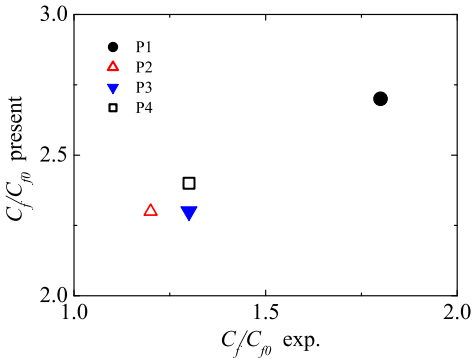

Figure 7: Comparison of friction increase ratio.

4. Conclusions

To predict rough wall turbulence without resolving rough geometry, spatial and Reynolds (double) averaged equations are modelled based on the two-component limit (TCL) second moment closure. The double averaging operation to the Naiver-Stokes equation produces the additional terms, namely, double-averaged drag force and inhomogeneous correction terms. The double-averaged drag force is modelled as the Darcy-Forchheimer form with the model functions using the plane porosity and plane hydraulic diameter. Binomial expansion is applied to model the effects of fluctuating velocity on the double-averaged drag force. The influence of the drag force on a pressure-strain term is modelled with Two-Component Limit constraints. The developed model is calibrated in turbulence over randomly distributed semi-spheres and spray paint surfaces. Comparison with the DNS results in turbulence over randomly distributed semi-spheres confirms that the modifications of the skin friction coefficient is well predicted and the Reynolds stress anisotropy near the rough wall is reasonably reproduced. Through validation in turbulence over spray paint surfaces, the present model is found to successfully predict the Reynolds number dependence of the roughness function in the fully rough regime. Furthermore, qualitative agreement of the skin friction increasing with the experimental data is confirmed.

5. Acknowledgements

A part of this study was financially supported by the research grants (No.17K14591 · 16K14162) of the JSPS Japan. The spray marine paint rough surfaces were supplied from Chugoku Marine Paints, Ltd. We would like to thank Mr. H. Mieno and Mr. H. Okimoto for their collaborations.

References

1. Taylor et al., Prediction of Turbulent Skin Friction for Two-Dimensional, Rib-Type Surface Roughness Using a Discrete Element Approach, *Mississippi State Univ. Mississippi State Engng. Ind. Res. Sta.*, 1985.
2. Christoph, G.H., Pletcher, R.H., Prediction of rough-wall skin friction and heat transfer. *AIAA J.* 21, pp. 509-515,1983.
3. Durbie, P.A. et al., Rough Wall Modification of Two-Layer $k-\varepsilon$, *Trans. ASME J. Fluid engng.* , Vol.123, pp.16–21, 2001.
4. Aupoix, B., Spalart P. R., A new extension for $k\omega$ turbulence models to account for wall roughness *Int. J. Heat Mass Transfer*, Vol.30, pp.54–65, 2000.

5. Aupoix, B., Spalart P. R., Extensions of the SpalartAllmaras turbulence model to account for wall roughness, *Int. J. Heat Mass Transfer*, Vol.24, pp.454–462, 2003.
6. Nikuradse, J., Laws of flow in rough pipes, NACA Technical Memorandum 1292, 1933.
7. Nakayama, A., Kuwahara, F., A macroscopic turbulence model for flow in a porous medium, *J. Fluids Eng.*, Vol.121, pp.427–433, 1999.
8. Pedras, M.H.J., de Lemos, M.J.S., Macroscopic turbulence modeling for incompressible flow through undeformable porous media, *Int. J. Heat Mass Transfer*, Vol.44, pp.1081–1093, 2001.
9. Kuwata, Y., Kawaguchi, Y., *Int. J. Heat Fluid Flow*, submitted.
10. Getachew, D., et al., A modified form of the $k - \varepsilon$ model for turbulent flows of an incompressible fluid in porous media. *Int. J. Heat Mass Transfer*, Vol.43, pp.2909–2915, 2000.
11. Craft, T.J., Launder, B.E., Principles and Performance of TCL-Based Second-Moment Closures *Flow. Turb. Combust.*, Vol.66, pp.355–372, 2001.
12. Craft, T.J., Launder, B.E., A Reynolds stress closure designed for complex geometries, *Int. J. Heat Fluid Flow*, Vol.17, pp.246–254, 1996.
13. Gunji, M., et al., Proposal and Verification of Estimation Method for Turbulent Frictional Drag of Irregularly Roughened Surface From the Roughness Curve Measurement, Proc. ASME FEDSM2016-7728, 2016.